NORTHERN CALIFORNIA CHAPTER
AMERICAN ASSOCIATION *of* PHYSICISTS IN MEDICINE

Young Investigators Symposium
May 31, 2019: 10:30AM – 6PM

at the

University of California at Berkeley, Hearst Memorial Mining Building 209

AGENDA

10:30AM Sign-In & Registration

11AM-12:30: Meet & Mingle at Lunch

12:30-1:30PM **"Harnessing the Innate Immune System for Cancer Therapy"**
Invited Keynote Speaker:
Eva Schmid, PhD, Research Scientist, Department of Bioengineering and Biophysics
University of California at Berkeley

Eva Schmid is a research scientist in the Bioengineering Department at UC Berkeley. She combines cell biology with bottom-up membrane reconstitution to gain insights into how immune cells interact with target cells, and to probe if they can be engineered for better tumor recognition.

1:30-2:10PM **PRESENTATIONS (Part I): *GRADUATE/UNDERGRAD STUDENTS*:**

1. Magnetic Particle Imaging for Lung Imaging and White Blood Cell Imaging, Xinyi Zhou (UC Berkeley)

2. "Motion monitoring with a stereo-vision surface imaging system for non-isocentric and noncoplanar treatment**,** Sergey Gasparyan (UCSC)

2:10PM 5 min BREAK/JUDGES CONFER

2:15-3:15 **PRESENTATIONS (Part II): *POST-DOCTORAL SCHOLARS*:**

3. "In vivo real-time tracking of single cells in whole-body PET/CT**,** Kyung Oh PhD (Stanford)

4. "Nanowire arrays restore vision in blind mice, Jing Tang (Stanford)

5. "Preliminary Trials of *In Vitro* Circulating Tumor Cell Cluster Tracking with the Mini-EXPLORER II Total-Body PET/CT Scanner, Qian Wang (UC Davis)

3:15-3:45PM – REFRESHMENTS SERVED - (JUDGES CONFER)

3:45-4:45PM **PRESENTATIONS (Part III): *MEDICAL PHYSICS RESIDENTS***

6. Evaluation of Off-axis Spatial Accuracy using an Integrated Quality Assurance Phantom for Frameless Single-isocenter Multitarget Stereotactic Radiosurgery**,** Dante P.I. Capal PhD (Stanford)

7. Voxel-specific proton stopping power ratios and uncertainties in a CT/MRI tissue classification model, A. Witztum (UCSF)

8. A Practical Quantitative MRI: The Radial TSE T2 Mapping with "Pseudo" Golden Ratio Reordering, Yutaka Natsuaki, PhD (UCSF)

5:00-5:30PM **SLAM COMPETITION (3 min presentations)**

- **Winner of the SLAM will represent the Northern California chapter at the AAPM Annual meeting in San Antonio, Texas, July 15, 2019**

5:30PM JUDGES CONFER / REFRESHMENTS SERVED
ANNOUNCEMENT OF AWARDS
TO FOLLOW: TOUR UC Berkeley BME

Northern California Chapter of the AAPM – Young Investigators Symposium, May 31, 2019

ALL Presentation Titles and Abstracts

UC Berkeley:

1. Magnetic Particle Imaging for Lung Imaging and White Blood Cell Imaging, Xinyi Zhou (UC Berkeley)

Abstract: Magnetic particle imaging (MPI) is an emerging ionizing radiation-free biomedical tracer imaging technique that directly images the intense magnetization of superparamagnetic iron oxide nanoparticles (SPIOs). MPI offers ideal image contrast because MPI shows zero signal from background tissues. Moreover, there is zero attenuation of the signal with depth in tissue, allowing for imaging deep inside the body quantitatively at any location. I discuss my dissertation work on two projects that take advantage of these characteristics of MPI, lung ventilation/perfusion (V/Q) imaging and white blood cell (WBC) tracking towards infection imaging. V/Q imaging is essential for diagnosing the common and life-threatening condition of pulmonary embolism, but traditional scintigraphy methods are slow due to the need for radionuclide prep. WBC imaging with scintigraphy has significant impact on clinical care for suspected osteomyelitis, but the 1-2 days needed for WBCs to localize to areas of infection means that image quality will have degraded due to radioactive decay. I show that MPI can offer similar tracer images without the disadvantages of radionuclides.

Stanford University

2. In vivo real-time tracking of single cells in whole-bodyPET/CT

Kyung Oh Jung,Tae Jin Kim, Byunghang Ha,and Guillem Pratx
Department of Radiation Oncology, Division of Medical Physics, Stanford University School of Medicine, Palo Alto, California, USA.

Objectives: With the progress in cell-based therapies, molecular imaging methods are increasingly being used for *in vivo*cell-tracking applications. They are also being applied to study various physiological and pathological processes, such as stem cell homing and cancer metastasis. Due to its high sensitivity and clinical applicability, positron emission tomography (PET) is the ideal modality for tracking cells. The purpose of this research is to demonstrate that, contrary to common knowledge, PET has sufficient sensitivity to track the migration of single cells in mice, in real-time and at the whole-body level.
Methods: To enable PET tracking, human breast cancer cells (MDA-MB-231) were passively labeled with ^{68}Ga-labeled mesoporous silica nanoparticles(MSNs). Using fluorescence microscopy, a small number of single cells were isolated in a 96-well plate through a statistical process of limiting dilution, and their radioactivitywasquantified by radioluminescence microscopy (RLM) and gamma counting. Finally, single cells were tracked both in phantoms and healthy mice using a small-animal PET/CT scanner (Inveon). A helical phantom was constructed by coiling a length of tubing around a 3D-printed cylinder (51 mm diameter, 27 mm helical pitch). List-mode data were acquired while a single cell was circulated through the phantom. Healthy mice were injected both intravenously (tail-vein) and in the foot pad, then they were moved to the PET scanner for real-time tracking. Real-time tracking was achieved by placing a catheter in the mouse tail vein. Finally, list-mode data were reconstructed using both conventional OSEM and a custom spatiotemporal trajectory reconstruction algorithm. The 3D trajectoryof single cells was analyzed in terms of velocity and accuracy.CT images were acquired for anatomical reference.
Results: Radioactivity was 30 Bq/cell on average, with a range of 0-110 Bq/cell. RLM imaging confirmed uptake of 68Ga-MSNs by single cells but suggested heterogeneous distribution of the 68Ga-MSN label. The specificity of the radiolabeling was confirmed by verifying that the radioactivity of a single cell cannot be split into multiple vials. Higher-radioactivity cells were then tracked using PET, both in phantom and in mice. A single cell (67 Bq) moving through thehelical phantom at 1.36 mm/s was tracked in real-time with accuracy better than 5 mm (root-mean-square error). Its velocity was estimated and found to be consistent with the flow rate in the tubing. *In vivo*experiments were also conducted in mice. Single cells injectedIVwere located in the lungs;those injected in the footpad remained at the injection site, with no detectable motion. Finally, the migrationof a single cancer cell was trackeddynamicallyusing a spatiotemporal trajectory reconstruction algorithm. The single cell reached its final destination in the lungs 2-3 seconds after tail-vein injection.Itsaveragevelocity was estimatedat around 40 mm/s, consistent with blood flow rate.
Conclusions: Single breast cancer cellsweresuccessfully labeled with 68Ga-MSNsand tracked using PET/CT, both in a phantom and *in vivo*in mice. This is the first demonstration of PET imaging and real-time tracking of radiolabeled single cells*in vivo*. This new platform for single-celltrackingcould be used to determine the kinetics of cell trafficking and arrest during the earliest phase of the metastatic cascade, the trafficking of immune cells during cancer immunotherapy, or the distribution

3. Evaluation of Off-axis Spatial Accuracy using an Integrated Quality Assurance Phantom for Frameless Single-isocenter Multitarget Stereotactic Radiosurgery

Dante P.I. Capaldi1, Lawrie Skinner1, Piotr Dubrowski1, Amy S. Yu1
1Department of Radiation Oncology, Stanford University School of Medicine, Stanford,

Purpose: The off-axis accuracy of the linear accelerator is crucial for single-isocenter multitarget stereotactic-radiosurgery (SRS). The common Winston-Lutz test is limited to only evaluating accuracy at the isocenter. In this study, a novel quality-assurance (QA) phantom was developed and validated to evaluate off-axis accuracy (i.e. off-axis Winston-Lutz test) to facilitate implementation of a frameless single-isocenter, multitarget SRS program.
Methods: A row of off-axis ball-bearings (BBs) was designed and integrated into a novel 3D printed QA phantom with the ability to QA various positioning systems as well as quantifying dosimetric accuracy. A CT scan of the phantom was acquired, digitally reconstructed radiographic images were generated, and portal images were delivered on a Varian Truebeam with a high-definition multi-leaf-collimator (MLC). To quantify the spatial-accuracy versus distance from isocenter, 2D displacements were calculated between the planned and delivered BB locations relative to their respective MLC defined field boarders. The results for the central BB was validated against commercial software. Furthermore, the phantom was physically shifted by known amounts (0mm, 0.5mm, and 1.0mm) and images were analyzed to determine whether the shifts were identified. Univariate-regression analysis (Pearson correlation coefficient [r]) was performed to quantify relationships.
Results: The proposed QA phantom identified a reduction in spatial-accuracy further away from isocenter. Differences increased as distance from isocenter increased (slope=0.01±0.17;r=0.90;p=0.03) exceeding recommended SRS accuracy tolerances at 7cm away from isocenter. To validate, the average difference between our analysis and commercial Winston-Lutz software was less than 0.02mm for the central BB. Additionally, known shifts of the phantom were accurately identified (slope=1.10±0.13).
Conclusion: The spatial accuracy of a linear accelerator versus distance from isocenter was evaluated using a novel integrated QA phantom. With the ability to quantify off-axis spatial-discrepancies, we can determine limitations on the maximum distance between targets to ensure a single-isocenter multitarget SRS program meets recommended guidelines. I
nnovation/Impact: With the recent advances in radiation oncology, such as those presented in the SABR-COMET clinical trial (Palma et al., Int.J. Radiat. Oncol. Biol. Phys., 2018), there will be an imminent increase in the number of multitarget SRS treatments for patients that would have otherwise been treated with palliative standard of care therapies alone. As a result, implementation of a frameless linear accelerator VMAT based single-isocenter, multitarget cranial SRS program would improve efficiency by reducing overall treatment times and increase patient's comfort (Clark et al., Int. J. Radiat. Oncol. Biol. Phys., 2010). Commissioning multitarget frameless single-isocenter SRS requires a rigorous QA program - specifically designed to quantify the spatial accuracy of a linear accelerator (Winston-Lutz test) as a function of distance from the isocenter (Stanhope et al., Pract. Radiat. Oncol., 2012). The phantom we designed and developed will facilitate the translation of multitarget frameless VMAT radiosurgery techniques. Furthermore, the proposed phantom has the ability to QA kV, MV, CBCT, and surface image-guidance systems for frameless treatments which provide greater patient comfort with an open-faced mask and faster treatment times (Yu et al., Med. Phy., 2018).
Key Results: Figure 1 illustrates the design and development of a prototype phantom to quantify the spatial accuracy of a linear accelerator as a function of distance from the isocenter. Figure 2 (C) shows the spatial accuracy as a function of distance from the isocenter, illustrating that the spatial accuracy reduces further away from isocenter. Furthermore, we tested the robustness of the analysis – where we physically shifted the phantom a known amount and recovered the offset in analysis pipeline (Figure 2 [D]).

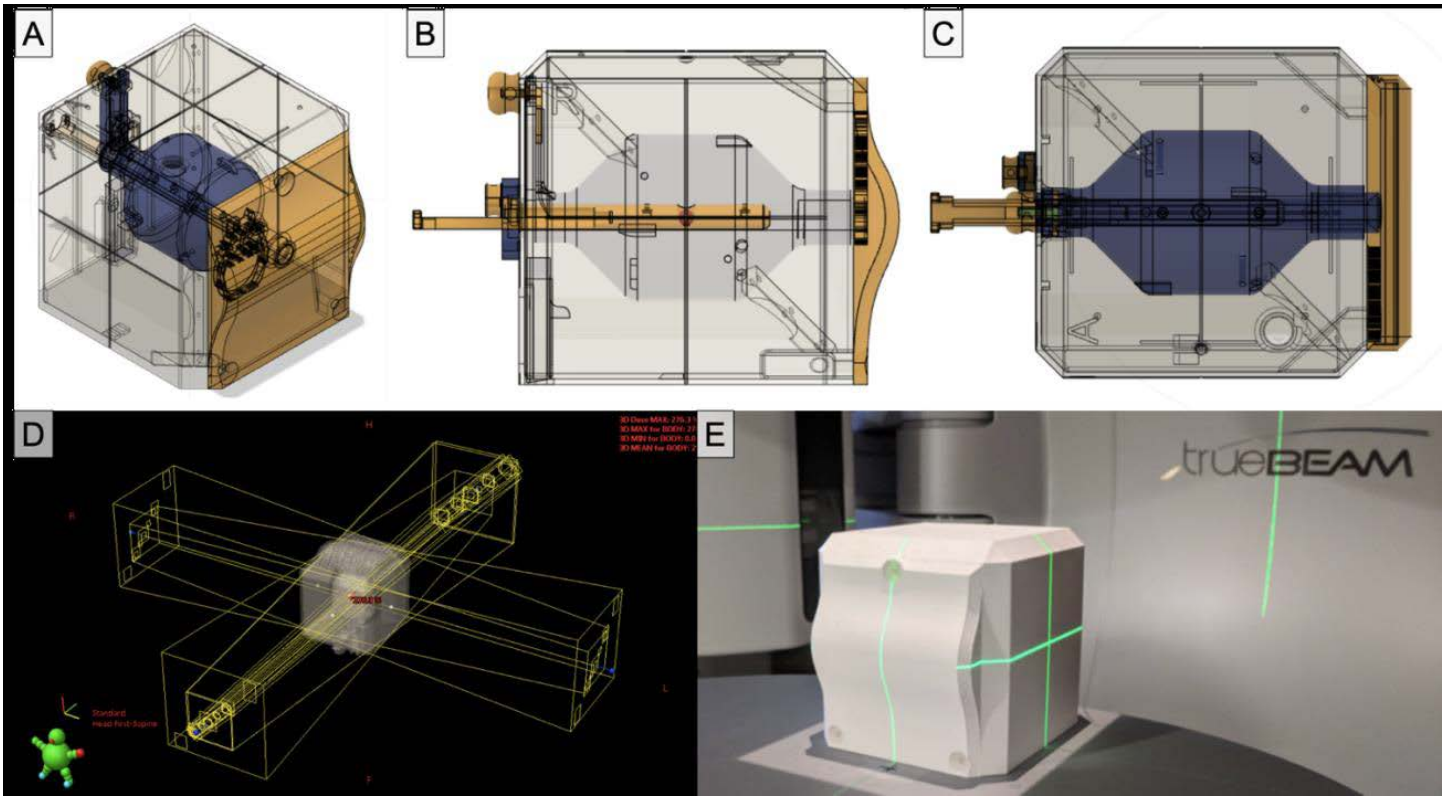

Figure 1. Design and development of a QA phantom to quantify the spatial accuracy of a linear accelerator-based single-isocenter, multitarget cranial radiosurgery system (**A-C**). (**D**) Eclipse treatment plan portal fields. (**E**) 3D printed QA phantom on Varian Truebeam (Varian Medical Systems, Palo Alto, CA).

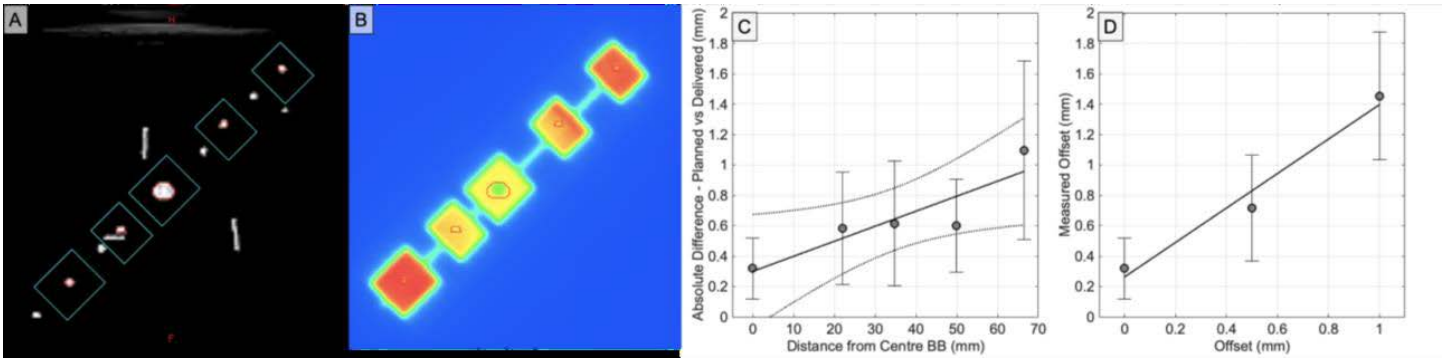

Figure 2. The results of the phantom with a representative planned field (**A**) vs delivered field (**B**) as well as the quantitative Winston-Lutz 2D displacements (**C**) for off-axis BB locations (slope=0.01±0.17, r=0.90, p=0.03) and (**D**) demonstrating the robustness of the analysis by shifting the phantom and recovering the shifts (offsets) (physical offset vs measured offset, slope=1.10±0.13). Points = mean; error-bars = standard-deviation; line = linear-regression; dotted-lines = 95% confidence-interval.

4. Nanowire arrays restore vision in blind mice

Jing Tang, Postdoctoral Scholar, Prof. Yi Cui Group

The restoration of light response with complex spatiotemporal features in retinal degenerative diseases towards retinal prosthesis has proven to be a considerable challenge over the past decades. Herein, inspired by the structure and function of photoreceptors in retinas, I develop artificial photoreceptors based on gold nanoparticle-decorated titania nanowire arrays, for restoration of visual responses in the blind mice with degenerated photoreceptors. Green, blue and near UV light responses in the retinal ganglion cells (RGCs) are restored with a spatial resolution better than 100 µm. ON responses in RGCs are blocked by glutamatergic antagonists, suggesting functional preservation of the remaining retinal circuits. Moreover, neurons in the primary visual cortex respond to light after subretinal implant of nanowire arrays. Improvement in pupillary light reflex suggests the behavioral recovery of light sensitivity. My study will shed light on the development of a new generation of optoelectronic toolkits for subretinal prosthetic devices. Through pharmacological, optical, and electrical toolsets, I aim to develop effective therapeutic solutions to neurological disease states. These results, along with a discussion of future neural interfaces, aim to improve our understanding of the nervous system and to inform new therapeutic approaches for biomaterials and bioelectronics.

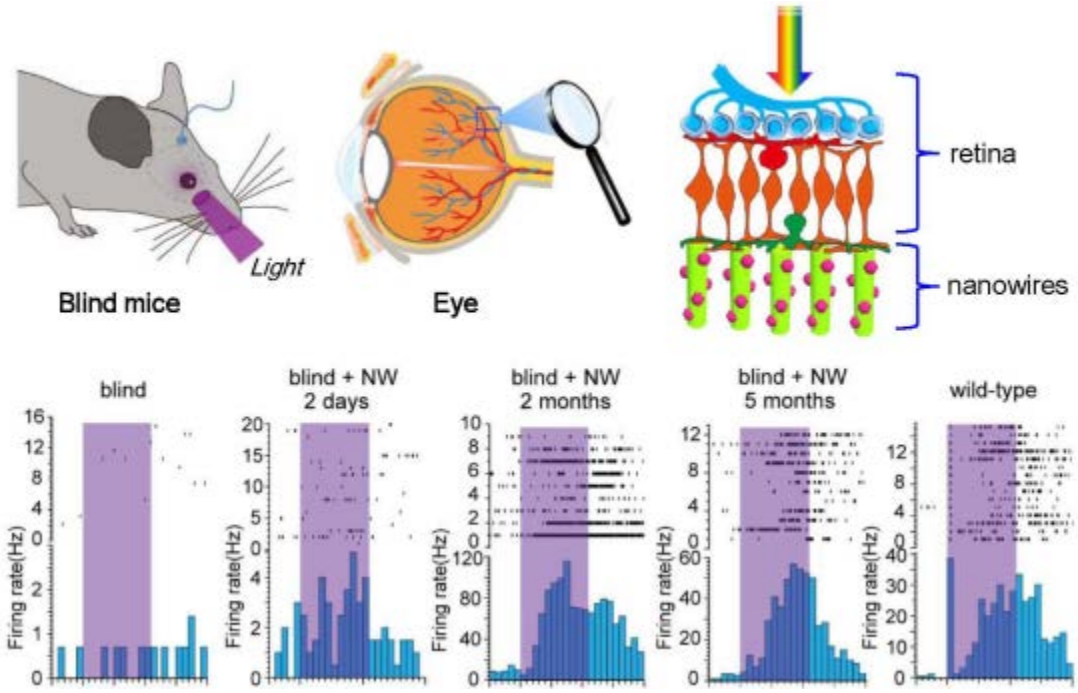

UC Davis

5. Preliminary Trials of *In Vitro* Circulating Tumor Cell Cluster Tracking with the MiniEXPLORER II Total-Body PET/CT Scanner

Qian Wang, Xuezhu Zhang, Simon R. Cherry
Department of Biomedical Engineering, University of California, Davis

An in-depth understanding of the mechanisms of cancer metastasis is critical for improving cancer diagnosis, prognoses and developing more effective therapies. The goal of this study is to develop a more effective strategy for *in vitro* cell tracking using the total-body PET/CT miniEXPLORER II scanner in order to help understand both static and dynamic characteristics of metastatic cells. Instead of using a single or a large number of cells, as is commonly done in cell tracking studies, we used radiolabeled tumor circulating cell (CTC) clusters to track cells. Aggregated CTCs, which are reported to avoid an immune response, have controllable sizes and provide an increased signal during imaging as compared to single cells, making them more stable and easier to be visualized. Prior to *in vitro* studies, the ability of miniEXPLORER II in capturing a dynamic low-activity cell-like source was assessed by imaging point sources with different activities (11-290 Bq) driven by a robot arm traveling in the PET field of view (FOV) at different speeds (0.4-4.8 cm/s). The results demonstrate miniEXPLORER II can track a point source of just ~10 Bq at low speeds (<1 cm/s), and 50 Bq at higher speeds. We then conducted trials on tracking single MDA-MB-231 cell clusters that were directly radiolabeled with [^{18}F]FDG and flowed through a helical tube of the phantom positioned at the center of the PET scanner. Two digital microscopes were installed at the inlet and outlet of the phantom to simultaneously monitor cell cluster flow and morphology. This preliminary data suggests that single cell clusters can be tracked *in vitro* with miniEXPLORER II. Based on the experience gained from this study, *in vivo* cell tracking of CTC clusters will be performed to further our understanding of cancer metastasis.

Supporting materials:

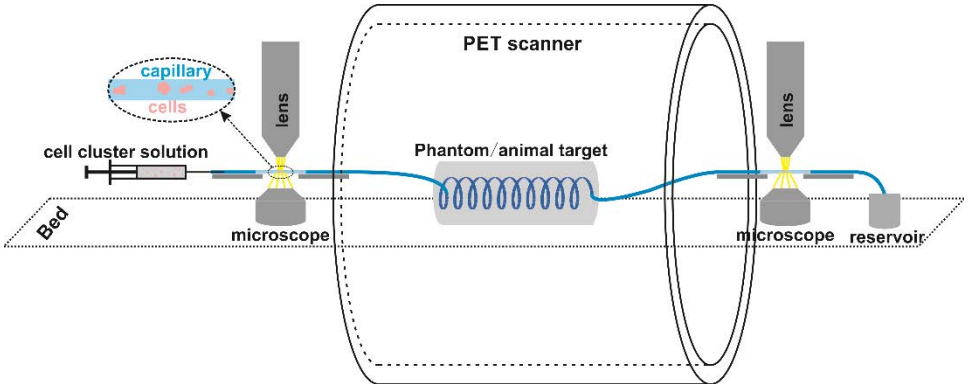

Figure 1. Sketch of dual-modal imaging platform for *in vitro* cell cluster tracking. The imaging platform includes the miniEXPLORER II scanner and two compact digital microscopes installed at the inlet and outlet of the phantom.

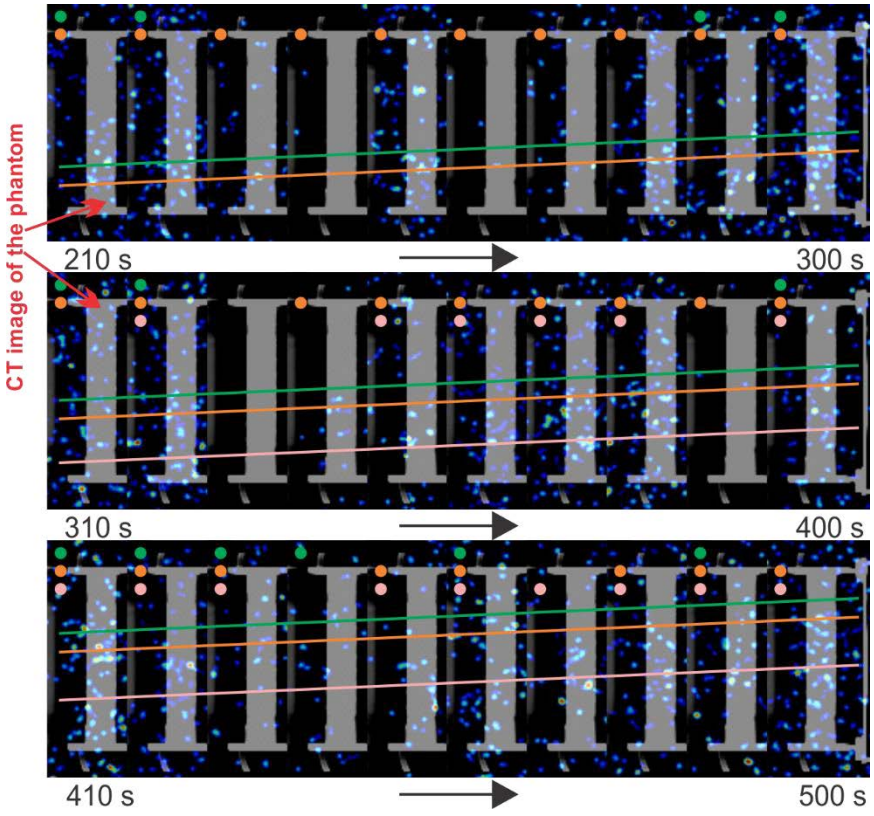

Figure 2. 30 consecutive PET images/frames for cell cluster tracking. These images have 10-s frame length and were fused with the phantom's CT image. 3 cell clusters were being tracked, along the orange, green and pink line. The reconstructed hot spots at different temporal frames of a cell cluster should fall along these lines. The dots on the upper left corner of each frame indicate whether the corresponding cell cluster was detected and localized in that frame or not.

UCSC

6. Motion monitoring with a stereo-vision surface imaging system for non-isocentric and noncoplanar treatment

Sergey Gasparyan, Lawrie B. Skinner, Amy S. Yu

Purpose: With the development of digital LINACs, radiation therapy with unconventional station point trajectory (e.g., non-coplanar beams and/or multiple isocenters) is emerging for the enhanced dosimetry and the efficient treatment. To monitor the patient during the treatment is challenging and one of the bottleneck problems in the clinical implementation. In current practice, due to the non-coplanar and non-isocentric beam arrangement, on board imaging system and in room x-ray system are no longer able to take the intra-fractional image to monitor patient. The optical surface monitor system, e.g., OSMS and C-RAD, requires manual couch angle input and might not be accurate due to the blind spot. The goal of this study is to develop a real-time monitoring technique for unconventional beam trajectories to ensure a safe and accurate treatment delivery with the camera on the couch to eliminate the blind spots.

Methods: Microsoft's Kinect stereo depth camera was mounted on the end of the couch to monitor the motion of the phantom (Fig. 1). The controlP5 library was used to create 3D surface point cloud of the object being tracked and depicting the region of interest. The software was written in processing 3 and involves a region and point class that were used by the main part of the software to track the phantom's motion. The accuracy of software was evaluated against the OSMS over known phantom displacements of length 3 mm, 5 mm, and 7 mm with placing a head phantom on the treatment couch.

Results: The tracking result between the proposed procedure and commercial system (OSMS) agree within 0.5 mm for all the direction. The summary of comparison between the proposed procedure and vendor's system are listed in Table 1.

Conclusion: We have designed and evaluated a motion tracking software with a camera mounted to the treatment table. By putting the depth sensor in the same frame of reference as the patient and eliminating the dead spots, we demonstrate a proof of concept that using surface registration and monitor the patient in real time is doable and safe for patient without additional radiation while the treatment table is moving during treatment.

Table 1	Lateral Shift			Superior/ inferior Shift		
n = 3	3 mm	5 mm	7 mm	5 mm	3 mm	7 mm
mean±SD, mm (Kinect)	2.42±0.10	4.95±0.11	6.52±0.30	4.64±0.08	2.70±0.13	7.00±0.19
mean±SD, mm (OSMS)	2.82±0.04	4.86±0.05	6.80±0.00	4.74±0.05	2.86±0.05	6.80±0.07
Delta, mm	0.40	-0.09	0.28	0.10	0.16	-0.20


e2v

UCSF

7. A Practical Quantitative MRI: The Radial TSE T2 Mapping with "Pseudo" Golden Ratio Reordering

Yutaka Natsuaki, PhD, Medical Physics Resident

Radiation Oncology, University of California San Francisco

Synopsis

The Radial TSE acquires TE data for T2 mapping in an efficient and motion robust fashion, but the choice of Echo Train Length (ETL) is limited. The current work introduces a novel view ordering algorithm that provides the necessary flexibility to the ETL, reducing the scantime significantly without a compromise.

Abstract

Purpose: The T2 quantification (T2 mapping) of the abdomen is challenging due to long scantime and respiratory motion. A technique called 2D radial TSE with tiered echo-sharing and bit-reverse (BR) view ordering can potentially resolve these issues by acquiring TE data for T2 mapping in an efficient and motion robust fashion, but imposes limits on the choice of Echo Train Length (ETL) due to the construction of BR. The current work introduces a novel view ordering algorithm with "pseudo" Golden Ratio (pGR) that removes the ETL restrictions. With pGR, the current 2D radial TSE can be further generalized to support any ETL and affording scan time reduction without a compromise in image and T2Map quality.

Methods: The proposed sequence and online reconstruction were implemented on a 3T scanner. The technique was validated with healthy volunteers (n=10) under a local IRB approved protocol. Radial TSE liver MRI data was acquired with (a) breath-hold liver protocol (pGR vs. BR) and (b) free-breathing liver protocol with diaphragm navigator (vs. the CartesianTSE counterpart). The resulting data sets were compared for overall image quality and for T2 quantitative values.

Results: With the pGR, the scan time of 2D radial TSE is reduced vs. the BR (by 18% in this study) without a compromise in image quality or T2Map values. Free-breathing optimized radial TSE generates scantime-efficient motion free images, while contrast and T2Map values matched the Cartesian counterpart.

Conclusion: Liver T2 mapping with motion robust and highly efficient 2D radial TSE technique has shown a great potential in the MR evaluation of the abdomen, and has the added benefit of providing quantitative T2 information. The pGR ordering scheme provides the necessary flexibility to bring the technique to routine clinical use and will play a future role in radiation oncology (e.g. MR machine-independent (e.g. regardless of different field strength or different vendors) quantitative T2 maps vs conventional arbitrary T2W Images, quantitative T2 parameter values as a novel input to the big data/machine learning for the cancer lesion delineations and recurrence predictions, etc.).

Innovation/Theory/Impact: For the 2D Radial TSE sequence with tiered echo-sharing and with Bit-Reverse (BR) view ordering, the angular sequence of the radial views $\boldsymbol{\theta}$ is calculated from the following equation:

$$\theta = \{[(m_i - 1) + (i-1)ET_N + (n-1)ETL]\Delta\theta\} mod\ \pi \quad ,$$

where *i* is the index for the echo number within an Echo Train Length (ETL), *n* is the index for the echo trains (TRs), ET_N is total number of echo trains rounded up to the nearest multiples of ETL, N is the total number of views, and $\Delta\theta = \pi/N$. m_i represents a corresponding *i-th* random integers in the range [1 ETL], in this case generated by BR (Fig.1). Due to its construction (i.e. binary digit), the BR can only allow ETL = power of 2.

We propose to replace the BR with the "pseudo" Golden Ratio (pGR) and redefine the first random integer term m_i in the range of [0 ETL-1]. The third term *(n-1)* is also replaced with pGR randomized number m_n in the range of [0 (N/ETL) -1] to promote the Golden Ratio view order for each echo, potentially reducing streaking artifacts in synthetic echo images (Fig.1). With this, ETL are no longer limited and now can freely

select any integers. In practice, ETL = 22~24 is optimal in terms of useful echo signals before the T2 relaxations decay.

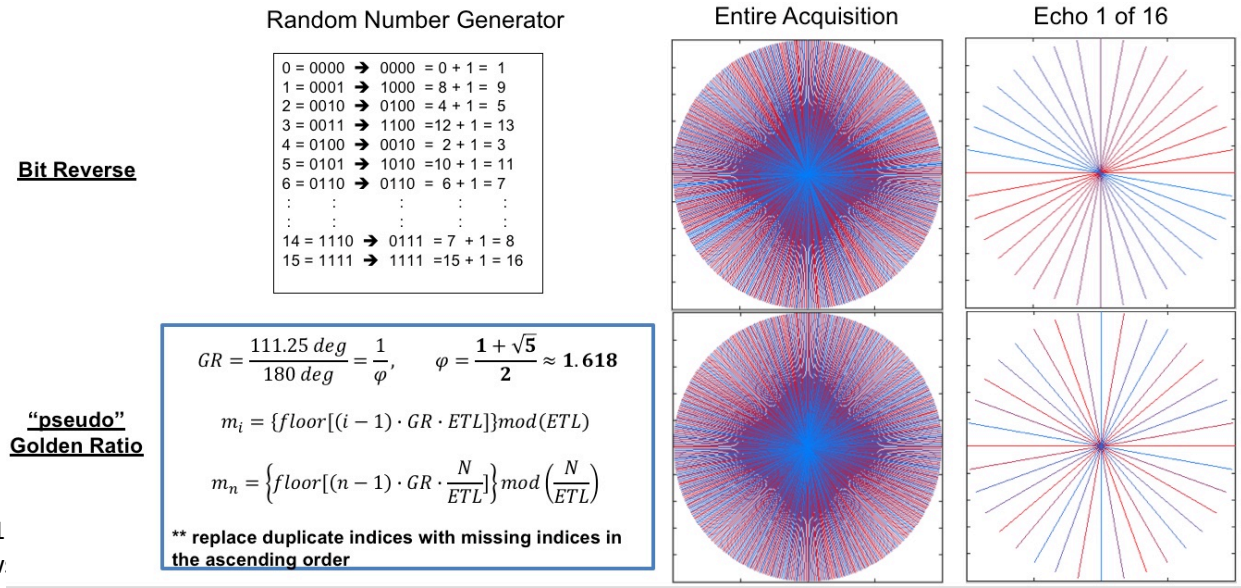

Fig.1 th 400 total view coverage.

Key Results: Fig. 2 shows the validation results from breath-hold protocol (BR vs pGR, no compromises in image quality and T2Map values despite 18% faster with pGR) and free-breathing hi-res protocol (Radial vs Cartesian, motion robust Radial vs motion artifacts across all Cartesian, but contrast/T2map values still matched).

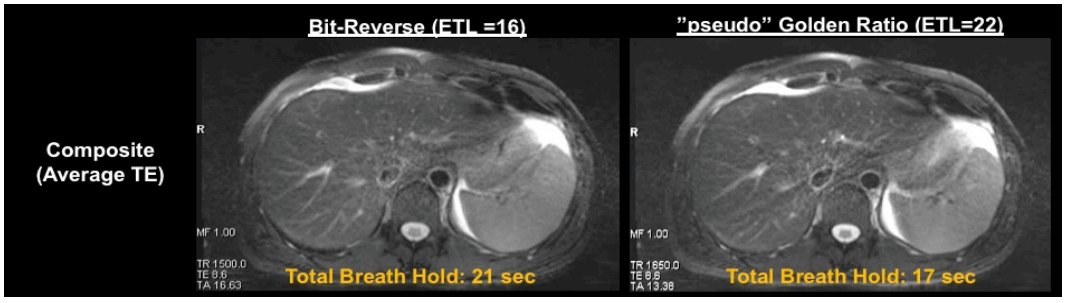

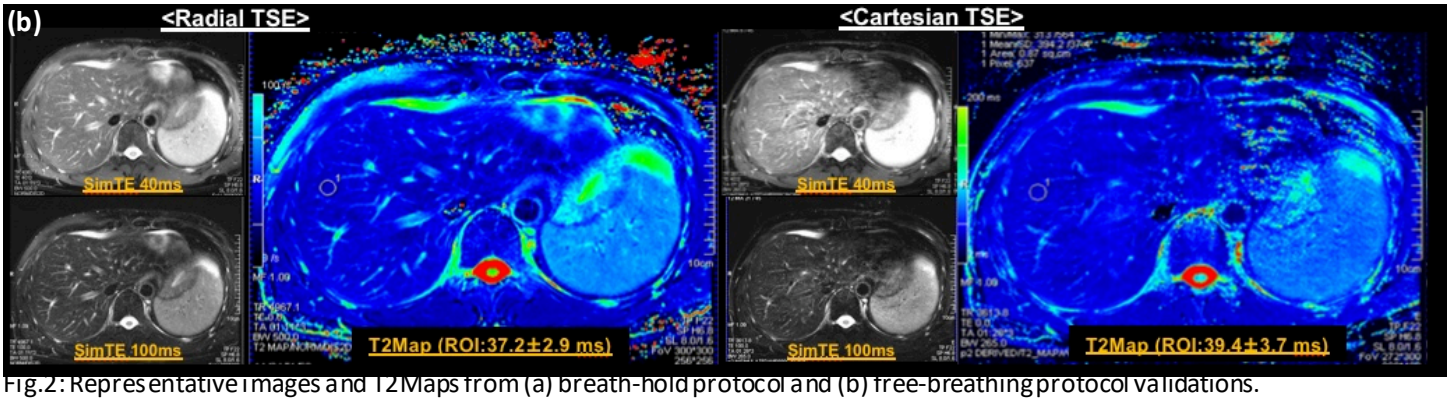

Fig.2: Representative images and T2Maps from (a) breath-hold protocol and (b) free-breathing protocol validations.

8. Voxel-specific proton stopping power ratios and uncertainties in a CT/MRI tissue classification model

Witztum, T.D. Solberg, A. Sudhyadhom
UCSF

Purpose:To create voxel-specific proton stopping power ratios (SPRs) and associated uncertainties based on a four-component tissue classification model using CT and MRI imaging.
Methods:The greatest source of uncertainty in the Bethe-Bloch equation (for SPR calculation) is the mean ionization potential (I_m). We propose a four-component classification (4CC) system whereby we classify molecules (or voxels) as proportions of water, fat, and protein (by MRI), and hydroxyapatite (HA) by CT. This model is written:

$$\ln(I_m) = (w_{water}\ln(I_{water})) + (w_{fat}\ln(I_{fat})) + (w_{protein}\ln(I_{protein})) + (w_{HA}\ln(I_{HA}))$$

where w is the mass content percentage and I is the mean ionization potential for each molecule. We have shown this model to calculate SPR within 0.2% of a summation over all elemental constituents (Bragg additivity rule).
The utility of this model is demonstrated by classifying every voxel on a pelvis CT slice as adipose, prostate, muscle, skin, stool, seminal vesicles, urine, cartilage, cortical bone, and trabecular bone. The 'true' 4CC composition (ICRP 23) of each class was used to create an SPR map. Errors were simulated with a normal distribution between 0-2% (water, HA) and 0-10% (fat) and randomized in +/- directions to mimic the errors in MRI/CT based classification. Protein was quantified as the remainder. Voxel SPR uncertainty (2 x standard deviation as percentage of SPR) and values for known CT imaging and range degradation errors are added in quadrature.
Results: A proton (E=250 MeV) SPR map was made along with an uncertainty map. The range of this uncertainty was 0.11-0.25% (quantification errors – Figure 1) and 0.63-0.67% (total – Figure 2).
Conclusion: Using the 4CC method is accurate and gives access to tissue composition specific SPR uncertainty. Once CT/MRI based content quantification techniques are introduced in radiotherapy, individual voxel SPRs and uncertainties should be considered in treatment planning systems. This is an area currently being investigated.

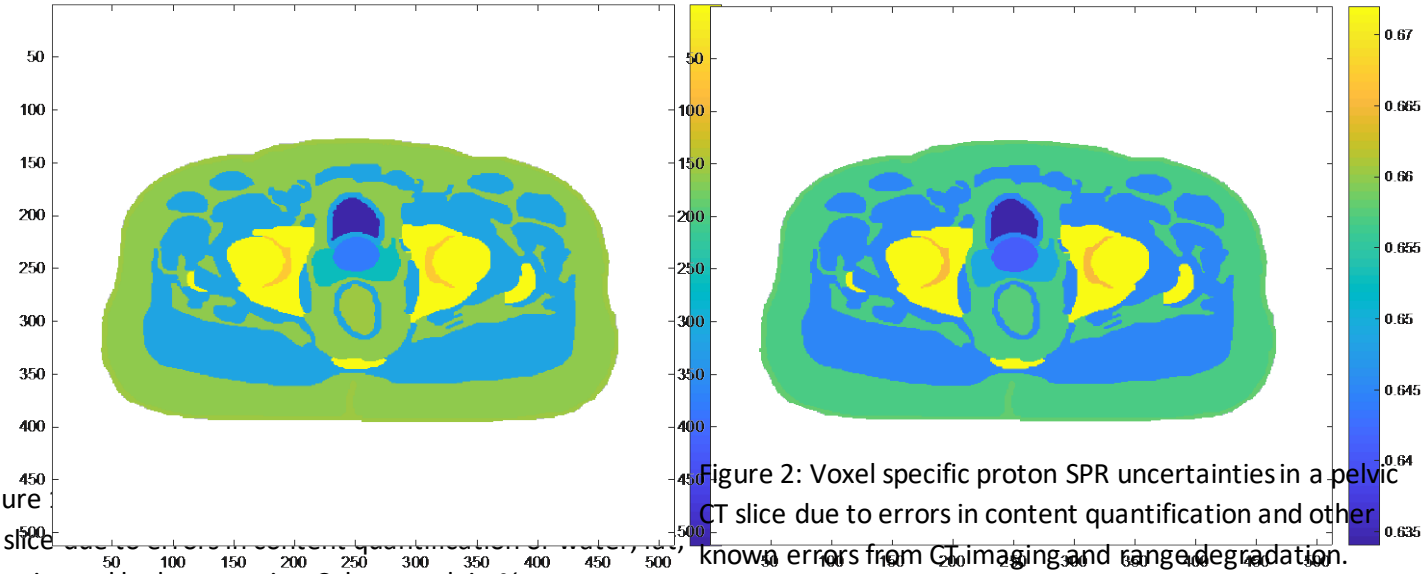

Figure 1: Voxel specific proton SPR uncertainties in a pelvic CT slice due to errors in content quantification of water, fat, protein, and hydroxyapatite. Colour wash in %.

Figure 2: Voxel specific proton SPR uncertainties in a pelvic CT slice due to errors in content quantification and other known errors from CT imaging and range degradation. Colour wash in %.